CMS Physics Analysis Summary

Contact: cms-pag-conveners-exotica@cern.ch 2018/02/27

Search for disappearing tracks in proton-proton collisions at $\sqrt{s} = 13\,\text{TeV}$

The CMS Collaboration

Abstract

A search is presented for long-lived charged particles that decay within the CMS detector and produce the signature of a disappearing track. A disappearing track is an isolated track with no associated hits in the muon detectors, little or no energy in associated calorimeter deposits, and missing hits in the outer layers of the silicon tracker. The search uses $38.4\,\text{fb}^{-1}$ of proton-proton collision data collected by the CMS detector in 2015 and 2016, at a center-of-mass energy of 13 TeV at the CERN LHC. The results of the search are interpreted in the context of anomaly-mediated supersymmetry breaking. The observation is consistent with the background-only hypothesis, and limits are set on the product of the cross section of direct chargino production and branching fraction to a neutralino and a pion in terms of the chargino mass and lifetime. At 95% confidence level, charginos with masses less than 715 GeV are excluded for a lifetime of 3 ns.

1 Introduction

This analysis summary presents a search for long-lived charged beyond-the-standard-model (BSM) particles that decay within the volume of the silicon tracker and produce the signature of a "disappearing track". A disappearing track is produced by a BSM charged particle whose decay products are undetected because they either have too little energy to be reconstructed or interact only weakly such that they do not produce hits in the tracker or deposit significant energy in the calorimeters.

Anomaly-mediated supersymmetry breaking (AMSB) [1, 2] is one of many BSM scenarios that would produce such a disappearing track. AMSB predicts a particle mass spectrum in which there is a small mass splitting between the lightest chargino ($\widetilde{\chi}_1^{\pm}$) and neutralino ($\widetilde{\chi}_1^0$), with the latter being the lightest supersymmetric particle (LSP). The chargino decays to a neutralino and a pion, $\widetilde{\chi}_1^{\pm} \to \widetilde{\chi}_1^0 \pi^{\pm}$. Because of the small chargino-neutralino mass splitting, the phase space for this decay is limited and as a consequence the chargino has a lifetime of order 1 ns. The pion from this decay has low momentum ($\approx$100 MeV), generally too low for the pion to be observable as a reconstructed track. If the chargino decays inside the tracker volume, it thus produces a disappearing track. We benchmark the search in terms of the chargino mass and lifetime in AMSB, although we note there are other BSM scenarios that produce the disappearing track signature [3–8].

Previous analyses by CMS and ATLAS have searched for disappearing tracks in proton-proton (pp) collision data at $\sqrt{s} = 8$ TeV [9, 10], and a recent analysis by ATLAS searched for short disappearing tracks in pp collision data at $\sqrt{s} = 13$ TeV [11]. The previous CMS search excluded at 95% confidence level (CL) direct electroweak production of charginos with a mass less than 505 GeV for a mean proper lifetime of 7 ns. Two significant improvements with respect to the 8 TeV search have been implemented for this search at 13 TeV: a new, dedicated trigger was developed specifically for this search, and also, the method used to estimate the background from standard model (SM) leptons has been modified to be fully determined from data, which makes the search more independent of the detector simulation.

2 The CMS detector

The central feature of the CMS apparatus is a superconducting solenoid of 6 m internal diameter. Within the solenoid volume are a silicon pixel and strip tracker, a lead tungstate crystal electromagnetic calorimeter (ECAL), and a brass and scintillator hadron calorimeter (HCAL), each composed of a barrel and two endcap sections. Forward calorimeters extend the pseudorapidity coverage provided by the barrel and endcap detectors. Muons are measured in gas-ionization detectors embedded in the steel flux-return yoke outside the solenoid.

The silicon tracker measures charged particles within the pseudorapidity range $|\eta| < 2.5$. It consists of 1440 silicon pixel and 15 148 silicon strip detector modules and is located in the 3.8 T field of the superconducting solenoid. For nonisolated particles with transverse momentum $1 < p_{\mathrm{T}} < 10$ GeV and $|\eta| < 1.4$, the track resolutions are typically 1.5% in p_{T} and 25–90 (45–150) μm in the transverse (longitudinal) impact parameter [12]. Isolated particles of p_{T} = 100 GeV emitted at $|\eta| < 1.4$ have track resolutions of 2.8% in p_{T} and 10 (30) μm in the transverse (longitudinal) impact parameter [12].

Events of interest are selected using a two-tiered trigger system [13]. The first level (L1), composed of custom hardware processors, uses information from the calorimeters and muon detectors to select events at a rate of around 100 kHz within a time interval of less than 4 μs. The

second level, known as the high-level trigger (HLT), consists of a farm of processors running a version of the full event reconstruction software optimized for fast processing, and reduces the event rate to around 1 kHz before data storage.

The particle-flow (PF) event algorithm [14] reconstructs and identifies each individual particle with an optimized combination of information from the various elements of the CMS detector. The energy of photons is directly obtained from the ECAL measurement, corrected for zero-suppression effects. The energy of electrons is determined from a combination of the electron momentum at the primary interaction vertex as determined by the tracker, the energy of the corresponding ECAL cluster, and the energy sum of all bremsstrahlung photons spatially compatible with originating from the electron track. The energy of muons is obtained from the curvature of the corresponding track. The energy of charged hadrons is determined from a combination of their momentum measured in the tracker and the matching ECAL and HCAL energy deposits, corrected for zero-suppression effects and for the response function of the calorimeters to hadronic showers. Finally, the energy of neutral hadrons is obtained from the corresponding corrected ECAL and HCAL energy.

A more detailed description of the CMS detector, together with a definition of the coordinate system used and the relevant kinematic variables, can be found in Ref. [15].

3 Data sets

This search uses pp collision data collected by the CMS detector at $\sqrt{s} = 13\,\text{TeV}$ during 2015 and 2016, which corresponds to an integrated luminosity of $38.4\,\text{fb}^{-1}$ [16, 17]. We consider the data collected during the two years as independent data sets. In addition, because of changes to the configuration of the trigger during the 2016 run, we consider separately two data-taking periods, which we call 2016A and 2016B, containing data taken earlier and later in the year, respectively. The separate run periods and the integrated luminosities to which they correspond are given in Table 1.

Table 1: Data-taking periods considered as independent data sets for this search and the respective integrated luminosities to which they correspond.

Run period	Integrated luminosity [fb^{-1}]
2015	2.7
2016A	8.3
2016B	27.4

Simulated signal events of $\text{pp} \to \widetilde{\chi}_1^{\pm}\widetilde{\chi}_1^{\mp}$ and $\text{pp} \to \widetilde{\chi}_1^{0}\widetilde{\chi}_1^{\pm}$ are generated at leading order (LO) precision with PYTHIA 6.4.26 [18] with the CTEQ6L1 [19] parton distribution function (PDF) set for a variety of $\widetilde{\chi}_1^{\pm}$ masses and lifetimes, using sparticle mass spectra produced by ISAJET 7.80 [20]. The branching fraction for $\widetilde{\chi}_1^{\pm} \to \widetilde{\chi}_1^{0}\pi^{\pm}$ is set to 100% and $\tan\beta$ is fixed to 5 with $\mu > 0$. These events are normalized using chargino production cross sections calculated at next-to-leading order (NLO) plus next-to-leading-log (NLL) precision using RESUMMINO [21, 22] with CTEQ6.6 [23] and MSTW2008nlo90cl [24] PDF sets, where the ratio of $\widetilde{\chi}_1^{0}\widetilde{\chi}_1^{\pm}$ to $\widetilde{\chi}_1^{\pm}\widetilde{\chi}_1^{\mp}$ production is calculated to be roughly 2:1 across all chargino masses considered. Scale factors are applied as a function of the p_{T} of the sparticle pair (either $\widetilde{\chi}_1^{\pm}\widetilde{\chi}_1^{\mp}$ or $\widetilde{\chi}_1^{0}\widetilde{\chi}_1^{\pm}$) to correct for mismodeling of initial state radiation (ISR) in PYTHIA. These scale factors are derived by comparing experimental and simulated data in a $\text{Z} \to \mu\mu$ control region as a function of the p_{T} of the Z boson candidate, and are generally a correction of order +25% in the kinematic region relevant to this search.

Although the methods used to estimate backgrounds in this search are based on experimental data, samples of simulated SM processes are used to validate these methods and calculate systematic uncertainties. Drell–Yan events, single top quark production through the s and t channels, $Z\gamma$, $W\gamma$, and $W \to \ell\nu$ events, where ℓ can be an electron, muon, or tau lepton, are generated at NLO precision using the MADGRAPH5_AMC@NLO 2.3.3 generator [25, 26]. WZ, ZZ, and quantum chromodynamics (QCD) multijet events are generated at LO precision with PYTHIA 8.205 [27]. WW, $t\bar{t}$, tW, and $\bar{t}W$ events are generated at NLO precision using POWHEG v2.0 [28–32]. The fragmentation and hadronization for all simulated background processes is handled by PYTHIA 8.205. The NNPDF3.0 [33] PDF set is used for all simulated backgrounds, and the CUETP8M1 [34, 35] tune is used for the underlying event.

For both simulated signal and background events, the detector response is simulated with a full model of the CMS detector based on GEANT4 [36] and reconstructed with the same software as used for collision data. Simulated minimum bias events are superimposed on the hard interaction to simulate the effect of overlapping inelastic pp interactions within the same or neighboring bunch crossings, known as pileup, and the samples are reweighted to match the reconstructed vertex multiplicity observed in data.

4 Event selection

The search is performed on data events that pass one or more of several triggers with requirements on missing transverse momentum. We define the vector $\vec{p}_{\mathrm{T}}^{\,\mathrm{miss,\,no}\,\mu}$, with magnitude $p_{\mathrm{T}}^{\mathrm{miss,\,no}\,\mu}$, as the projection onto the plane perpendicular to the beam axis of the negative vector sum of the momenta of all reconstructed objects in an event with the exception of muons. The triggers require $p_{\mathrm{T}}^{\mathrm{miss,\,no}\,\mu}$ in L1. In the HLT, either $p_{\mathrm{T}}^{\mathrm{miss,\,no}\,\mu}$ or $p_{\mathrm{T}}^{\mathrm{miss}}$, defined similarly but with muons included in its calculation, is required. The lowest threshold of these triggers requires $p_{\mathrm{T}}^{\mathrm{miss,\,no}\,\mu} > 75\,\mathrm{GeV}$ as well as an isolated track with $p_{\mathrm{T}} > 50\,\mathrm{GeV}$ in the HLT. In the offline selection, only $p_{\mathrm{T}}^{\mathrm{miss,\,no}\,\mu}$ calculated from the full PF reconstruction is used. Events are required to have $p_{\mathrm{T}}^{\mathrm{miss,\,no}\,\mu} > 100\,\mathrm{GeV}$.

In signal events, $p_{\mathrm{T}}^{\mathrm{miss,\,no}\,\mu}$ is generated by an ISR jet recoiling off the sparticle pair. Jets are clustered from PF candidates using FASTJET 3.10 [37] with the anti-k_{T} algorithm [38] operated with a distance parameter of 0.4, and only jets with $p_{\mathrm{T}} > 30\,\mathrm{GeV}$ are considered in the analysis. Additional criteria are imposed on these jets to remove jets originating from calorimeter noise and misreconstructed leptons [39]. Events are required to have at least one jet with $p_{\mathrm{T}} > 110\,\mathrm{GeV}$ in order to be consistent with the ISR recoil topology.

We require the maximum difference in azimuthal angle $\Delta\phi_{\mathrm{max}}(\text{jet pairs})$ between any two jets to be less than 2.5 and the difference in azimuthal angle between the $\vec{p}_{\mathrm{T}}$ of the leading (highest energy) jet and $\vec{p}_{\mathrm{T}}^{\,\mathrm{miss,\,no}\,\mu}$ to be greater than 0.5. These requirements are designed to remove the large, reducible background originating from SM events composed of jets produced solely through the strong interaction, referred to as QCD multijet events. In these QCD multijet events, a dijet topology with back-to-back jets dominates and a significant $p_{\mathrm{T}}^{\mathrm{miss,\,no}\,\mu}$ typically comes from mismeasured jet energy. We refer to the selection up to this point, before any track-related criteria are imposed, as the "basic control region". The effect of the two main basic control region requirements on data and simulated signal and background events is shown in Fig. 1.

After the basic control region, candidate signal tracks are selected that have $p_{\mathrm{T}} > 55\,\mathrm{GeV}$ and

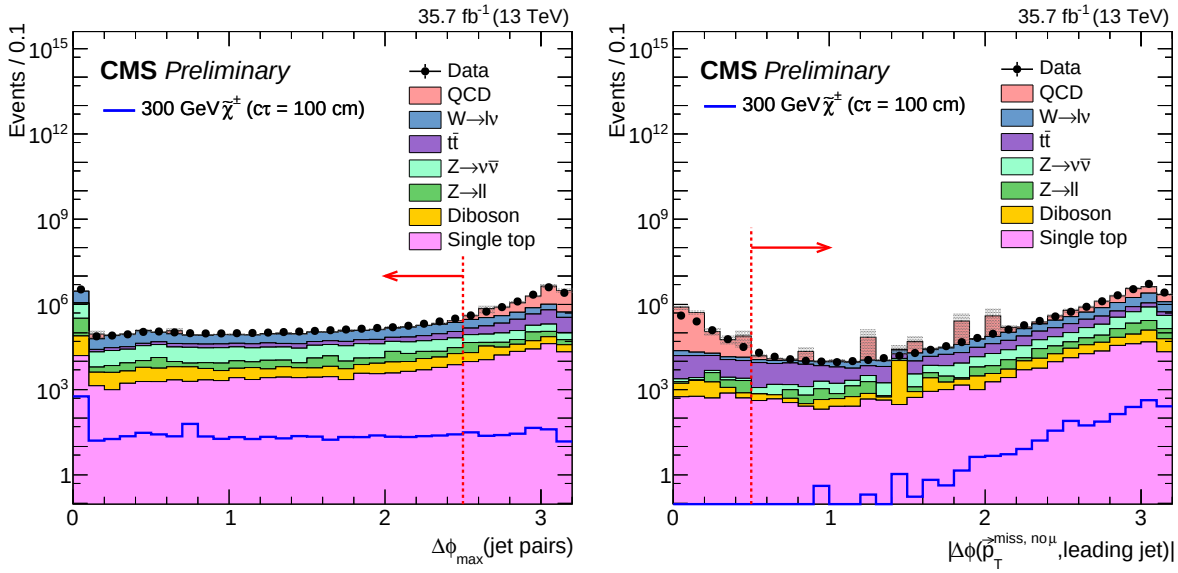

Figure 1: Distributions of the maximum difference in azimuthal angle between any two jets (left) and the difference in azimuthal angle between the $\vec{p}_{\mathrm{T}}$ of the leading jet and $\vec{p}_{\mathrm{T}}^{\,\mathrm{miss,\,no}\,\mu}$ (right) for events from the basic control region before either of the angular requirements on the jets or $\vec{p}_{\mathrm{T}}^{\,\mathrm{miss,\,no}\,\mu}$ are imposed. The blue lines show the distributions for simulated signal events with a chargino that has a lifetime of 100 cm/c and mass of 300 GeV, with a corresponding production cross section of 0.58 pb. The gray shaded area indicates the statistical uncertainty in the SM background, and the leftmost bin of the left plot includes events with only one selected jet. The red dashed lines indicate the chosen value for the requirement on each variable, and the arrows indicate which events are selected.

$|\eta| < 2.1$. We demand that candidate tracks be isolated from other activity in the tracker by requiring the scalar sum of the p_T of other tracks within a cone of $\Delta R = \sqrt{(\Delta\phi)^2 + (\Delta\eta)^2} < 0.3$ around the momentum vector of the candidate track be less than 5% of the p_T of the candidate track. Candidate tracks are also required to be well-separated from jets with $\Delta R(\text{track, jet}) > 0.5$.

One source of background for this search is "spurious tracks", i.e., pattern recognition errors that do not correspond to an actual charged particle. Spurious tracks can be missing hits in the outer layers of the silicon tracker and muon detectors, and are not generally associated to large energy deposits in the calorimeters, thus mimicking a disappearing track. This background is suppressed by requiring that candidate tracks have at least three hits in the pixel detector and at least seven hits overall in the tracker. A missing hit in a layer of the tracker between the interaction point and the first actual hit on the track is called a missing inner hit, while a missing hit between the first and last hits on the track is called a missing middle hit. We require candidate tracks to have no missing inner or middle hits. In other words, there must be a consecutive pattern of hits originating in the tracker layer closest to the interaction point. Since spurious tracks often appear displaced from the interaction point, we require for all tracks a transverse impact parameter $|d_0| < 0.02\,\text{cm}$ and a longitudinal impact parameter $|z_0| < 0.5\,\text{cm}$, both with respect to the primary vertex, defined as the reconstructed vertex with the largest value of summed physics-object p_T^2. The physics objects chosen are those that have been defined using information from the tracking detector, including jets, the associated missing transverse momentum, taken as the negative vector sum of the p_T of those jets, and charged leptons.

The other main source of background for this search is isolated charged leptons that are not correctly reconstructed by the PF algorithm. Leptons can have missing hits in the tracker for several reasons; for example, large bremsstrahlung in the case of electrons, or nuclear interactions with the tracker material in the case of hadronically decaying tau leptons. Leptons may also have small associated calorimeter energy deposits; for example, because of dead or noisy channels. To mitigate this background, events where candidate tracks are close to reconstructed leptons ($\Delta R(\text{track, lepton}) < 0.15$) are vetoed. In order to avoid leptons that fail to be reconstructed because of detector inefficiencies, we impose fiducial track criteria on the candidate tracks. We avoid regions of muon reconstruction inefficiency by vetoing gaps in the coverage of the muon chambers at $0.15 < |\eta| < 0.35$ and $1.55 < |\eta| < 1.85$. Similarly we avoid regions of electron reconstruction inefficiency by vetoing the overlap region between the barrel and endcap sections of the ECAL at $1.42 < |\eta| < 1.65$, as well as tracks within $\Delta R < 0.05$ of a dead or noisy ECAL channel, where ΔR is calculated with respect to the track momentum at the point of closest approach to the center of CMS. Additional areas of inefficiency are identified and rejected using electron and muon tag-and-probe studies, where $Z \to \ell\ell$ candidates are selected in data with $m_{\ell\ell} \approx m_Z$ and the Z resonance is exploited to obtain a sample of tracks that have a high probability of being leptons, without explicitly requiring them to be reconstructed as leptons.

Two additional requirements define the criteria for a track to "disappear". First, we require the candidate signal tracks to have at least three missing outer hits, which are missing hits in the tracker outside of the last hit on the track. Second, the associated calorimeter energy within $\Delta R < 0.5$ of the track momentum, E_{calo}, is required to be less than 10 GeV, where ΔR is calculated using the track coordinates at the point of closest approach to the center of CMS. These two quantities, missing outer hits and E_{calo}, are shown in Fig. 2 for simulated signal and background events passing the full selection except for the requirement on the variable being plotted. As can be seen, these variables are very effective at isolating the signal, as tracks from

background events typically have no missing outer hits and significant E_{calo}.

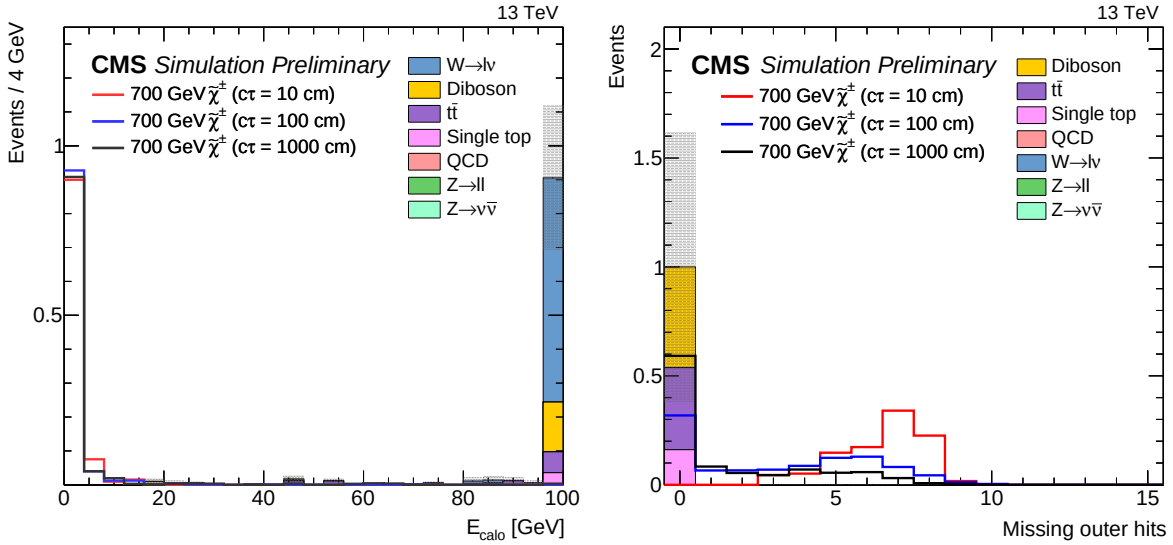

Figure 2: Distributions of E_{calo} (left) and number of missing outer hits (right) for tracks in simulation that pass the full selection except for the requirement on the variable being plotted. Each signal distribution and the sum of the SM background distributions are scaled to have unit area, and the rightmost bins include overflow entries. The gray shaded area indicates the statistical uncertainty in the SM background.

5 Background estimation

5.1 Charged leptons

The dominant source of high-p_{T}, isolated tracks from SM processes is charged leptons (electrons, muons, and hadronically decaying tau leptons) from the decay of W or Z bosons or virtual photons. In order for events with such tracks to enter the search region, three things must happen: (1) the lepton must fail to be reconstructed as such, while still leaving a track in the silicon tracker; (2) the resulting $p_{\text{T}}^{\text{miss, no}\,\mu}$ must be large enough for the event to pass the offline $p_{\text{T}}^{\text{miss, no}\,\mu}$ requirements; and (3) the resulting $p_{\text{T}}^{\text{miss}}$ and $p_{\text{T}}^{\text{miss, no}\,\mu}$ must be large enough for the event to pass the triggers.

The key point is that $p_{\text{T}}^{\text{miss}}$ and $p_{\text{T}}^{\text{miss, no}\,\mu}$ are affected by whether the lepton is reconstructed as a lepton or not. If the lepton is not reconstructed, its energy does not contribute to the visible energy of the event. The method used to estimate the background from charged leptons is based on calculating the probability in data of the three conditions listed above, with each lepton flavor treated independently.

The first probability we consider is P_{veto}, the probability that the lepton in a single lepton event is not reconstructed as such. For each flavor of charged lepton, we estimate P_{veto} using a tag-and-probe study. The electron (muon) tag-and-probe selections target $\text{Z} \to \text{ee}$ ($\text{Z} \to \mu\mu$) candidates. For this study we select events passing a single-electron (single-muon) trigger, and that contain a reconstructed electron (muon) that passes tight identification and isolation criteria. This lepton serves as the tag. A separate track, the probe, is then required that passes the disappearing track criteria, except for those defining the electron (muon) veto in Table 2. The tag

lepton and probe track are required to have an invariant mass within 10 GeV of the Z boson mass and to have opposite signs of electric charge.

Table 2: Definitions of the lepton vetoes used in the tag-and-probe studies to estimate P_{veto} for each flavor of charged lepton. The criteria listed are chosen from the search criteria as the most efficient to reject each flavor.

Flavor	Selection
Electron	Min $\Delta R_{\text{track,electron}} > 0.15$
	$E_{\text{calo}} < 10\,\text{GeV}$
	Missing outer hits ≥ 3
Muon	Min $\Delta R_{\text{track,muon}} > 0.15$
	Missing outer hits ≥ 3
Tau leptons	Min $\Delta R_{\text{track,had. tau lepton}} > 0.15$
	$\Delta R_{\text{track,jet}} > 0.5$
	$E_{\text{calo}} < 10\,\text{GeV}$
	Missing outer hits ≥ 3

For the tau lepton tag-and-probe study, we define two selections targeting $Z \to \tau\tau$ events that are combined for the calculation of P_{veto}: one where the electron from a $\tau \to e\nu\nu$ candidate is selected as the tag, and one where the muon from a $\tau \to \mu\nu\nu$ candidate is selected as the tag. These two selections are identical to the electron and muon tag-and-probe selections defined above, respectively, except for two modifications. First, we require the transverse mass $m_{\text{T}} = \sqrt{2p_{\text{T}}^{\ell} p_{\text{T}}^{\text{miss}}(1-\cos\Delta\phi)}$ to be less than 40 GeV, where p_{T}^{ℓ} is the magnitude of the transverse momentum of the tag lepton and $\Delta\phi$ is the difference in azimuthal angle between the $\vec{p}_{\text{T}}$ of the tag lepton and $\vec{p}_{\text{T}}^{\text{miss}}$. This m_{T} requirement is made to reduce contamination from W+jets events. Second, as the tau leptons from the Z decay are not fully reconstructed, the dilepton invariant mass requirement is $m_{\text{Z}} - 50 < m < m_{\text{Z}} - 15\,\text{GeV}$, where m_{Z} is the world-average mass of the Z boson [40].

For each of these selections, we also define a version in which the tag lepton and probe track are required to have the same sign of electric charge instead of opposite signs. This requirement makes the selected probe tracks unlikely to originate from a real particle, and these selections are used to subtract the background from spurious tracks in the calculation of P_{veto}.

For each of the three tag-and-probe channels (electrons, muons, and tau leptons), $N_{\text{T\&P}}$ ($N_{\text{T\&P}}^{\text{veto}}$) and $N_{\text{SS T\&P}}$ ($N_{\text{SS T\&P}}^{\text{veto}}$) are the numbers of selected tag-probe pairs before (after) the final lepton veto is applied to the probe tracks, for the opposite-sign and same-sign selection, respectively. From this, the veto probability is calculated as:

$$P_{\text{veto}} = \frac{N_{\text{T\&P}}^{\text{veto}} - N_{\text{SS T\&P}}^{\text{veto}}}{N_{\text{T\&P}} - N_{\text{SS T\&P}}}. \tag{1}$$

We define P_{offline} as the conditional probability of a single lepton event to pass the offline requirements of $p_{\text{T}}^{\text{miss, no}\,\mu} > 100\,\text{GeV}$ and $|\Delta\phi(\text{leading jet}, \vec{p}_{\text{T}}^{\text{miss, no}\,\mu})| > 0.5$ given that the lepton is not reconstructed as such. Using events in single lepton control regions in data, we introduce modified $\vec{p}_{\text{T}}^{\text{miss, no}\,\mu}$ variables that represent what $\vec{p}_{\text{T}}^{\text{miss, no}\,\mu}$ would look like if the lepton in these events were not reconstructed, assuming that if a lepton is not reconstructed then it contributes no visible energy to the event. In the single electron and single tau lepton control regions, we use $\vec{p}_{\text{T}}^{\text{miss, no}\,\mu} + \vec{p}_{\text{T}}^{\text{lepton}}$. For the single muon control region, we simply use $\vec{p}_{\text{T}}^{\text{miss, no}\,\mu}$ since the p_{T}

of all reconstructed muons is already excluded from its calculation. We then estimate P_{offline} by counting the fraction of events with $p_{\text{T}}^{\text{miss, no}\,\mu} > 100\,\text{GeV}$ and $|\Delta\phi(\text{leading jet}, \vec{p}_{\text{T}}^{\text{miss, no}\,\mu})| > 0.5$ after modifying $\vec{p}_{\text{T}}^{\text{miss, no}\,\mu}$ in this way.

We define P_{trigger} as the conditional probability of a single lepton event to pass the $p_{\text{T}}^{\text{miss}}$ and $p_{\text{T}}^{\text{miss, no}\,\mu}$ triggers used in the search given that the lepton is not reconstructed as such and the event passes the offline requirements of $p_{\text{T}}^{\text{miss, no}\,\mu} > 100\,\text{GeV}$ and $|\Delta\phi(\text{leading jet}, \vec{p}_{\text{T}}^{\text{miss, no}\,\mu})| > 0.5$. We estimate P_{trigger} similarly to the estimation of P_{offline} in the single lepton control regions, assuming that an unreconstructed lepton contributes no visible energy to the event and constructing the modified $\vec{p}_{\text{T}}^{\text{miss, no}\,\mu} + \vec{p}_{\text{T}}^{\text{lepton}}$ for electrons and tau leptons, using $\vec{p}_{\text{T}}^{\text{miss, no}\,\mu}$ for muons. The exception for P_{trigger} is that instead of constructing these quantities with offline reconstructed leptons, online objects are used from both the L1 trigger and the HLT. For each lepton selected in each of the single lepton control regions in data, we find the closest L1 trigger object and closest HLT object within $\Delta R < 0.1$ of the offline object. The $\vec{p}_{\text{T}}$ of these objects is then added to the nominal $\vec{p}_{\text{T}}^{\text{miss}}$, as calculated by the L1 trigger and HLT, respectively, and to the nominal $\vec{p}_{\text{T}}^{\text{miss, no}\,\mu}$ in the case of the HLT. This way, we can test, event by event, if the L1 trigger and HLT would have passed, given these modifications to the online $\vec{p}_{\text{T}}^{\text{miss}}$ and $\vec{p}_{\text{T}}^{\text{miss, no}\,\mu}$. The fraction of events passing the offline $p_{\text{T}}^{\text{miss, no}\,\mu}$ requirements according to the procedure used to calculate P_{offline} that also pass the $p_{\text{T}}^{\text{miss}}$ and $p_{\text{T}}^{\text{miss, no}\,\mu}$ triggers by the above procedure is then the estimate of P_{trigger}.

The product of the three probabilities defined above (P_{veto}, P_{offline}, and P_{trigger}) gives the probability of an event with a charged lepton to enter the search region. We use the single lepton control regions to estimate the total numbers of events in data containing each flavor of lepton, N_{ctrl}^{ℓ}, and obtain the estimated number of background events from charged leptons as:

$$N_{\text{est}}^{\ell} = N_{\text{ctrl}}^{\ell} P_{\text{veto}} P_{\text{offline}} P_{\text{trigger}}. \tag{2}$$

Closure tests were performed in samples of simulated background events and in the early 13 TeV data taken in 2015. Both tests proved the validity of the background estimation method.

5.2 Spurious tracks

The contribution of spurious tracks to the background is largely suppressed by the requirements on the impact parameters of the tracks and that the tracks be missing no inner or middle hits in the tracker. We estimate the residual contribution from this background using a control region of $\text{Z} \to \mu\mu$ events as a representative sample of SM events. Within this sample, we additionally require a track, separate from the muons coming from the Z candidate, that passes the track requirements of the search region except for the transverse impact parameter criterion, which we replace with a sideband selection, $0.02 < |d_0| < 0.1\,\text{cm}$, designed to enhance the likelihood that the tracks we select are spurious. In this way, we can estimate the probability of spurious tracks that satisfy these requirements. This probability is multiplied by a transfer factor to obtain the probability of spurious tracks passing the nominal impact parameter requirement, P_{spurious}. This transfer factor is obtained from a sample of 3-hit tracks, to ensure that the d_0 distribution of spurious tracks is being sampled, without significant risk of contamination from tracks originating from actual charged particles. The estimated background from spurious tracks is the number of events in data in the basic control region, $N_{\text{ctrl}}^{\text{basic}}$, multiplied by P_{spurious}:

$$N_{\text{est}}^{\text{spurious}} = N_{\text{ctrl}}^{\text{basic}} P_{\text{spurious}}. \tag{3}$$

6 Systematic uncertainties

6.1 Background estimation

The lepton background estimates rely on the assumption that when a lepton is not reconstructed as such, it contributes no visible energy to the event. We test the impact of this assumption by replacing the nominal $\vec{p}_{\text{T}}^{\text{miss, no}\,\mu} + \vec{p}_{\text{T}}^{\text{lepton}}$ variable used to calculate P_{offline} and P_{trigger} with a "scaled down" version,

$$\vec{p}_{\text{T}}^{\text{miss, no}\,\mu} + \frac{p_{\text{T}}^{\text{lepton}} - 10\,\text{GeV}}{p_{\text{T}}^{\text{lepton}}} \vec{p}_{\text{T}}^{\text{lepton}}, \tag{4}$$

and recalculating P_{offline} and P_{trigger}. In other words, we assume that unreconstructed leptons contribute 10 GeV of visible energy to the event. The value of 10 GeV is chosen because candidate tracks are required to have $E_{\text{calo}} < 10\,\text{GeV}$ in the disappearing tracks search region. The difference from unity of the ratio

$$\frac{(P_{\text{offline}} P_{\text{trigger}})_{\text{scaled down}}}{(P_{\text{offline}} P_{\text{trigger}})_{\text{nominal}}} \tag{5}$$

is taken as the systematic uncertainty. This uncertainty is approximately 12 (17)% for electrons (tau leptons) and is not calculated for muons, since even successfully reconstructed muons are not expected to contribute substantial visible calorimeter energy to an event.

We assign a systematic uncertainty associated with the particular choice of the d_0 sideband region used to estimate the spurious track background. This is evaluated using the maximum variations in the background estimate as the lower bound on the sideband is increased from 0.02 cm to 0.1 cm. Maximum variations of 100% down and 45% up are seen for the 2016 data. For the 2015 data, since the estimate is zero and no indication of behavior different from 2016 data is observed, we assign a systematic uncertainty of 50% on this period. To apply systematic uncertainties to estimates of zero events, the recommendations of Ref. [41] are followed.

A systematic uncertainty associated with the evaluation of the sideband transfer factor using 3-hit tracks is determined. This systematic uncertainty is evaluated by examining the variation in the d_0 distribution going from tracks with three hits to at least seven hits using tracks in simulated events that are not associated with a generated particle. In this way, we can see how much the true distribution of d_0 for spurious tracks varies with the number of hits, and constrain the impact this variation has on the background estimate. This procedure yields an uncertainty of approximately -50% and $+100\%$ on the spurious track background estimate.

The spurious track background estimate rests on the assumption that the spurious track probability is similar between the $Z \to \mu\mu$ and basic control regions. However, there is nothing about the method used to calculate the spurious track background that prevents us from performing it in the basic control region. Thus, we are able to compare the estimate we obtain from these two independent control regions. This comparison serves to validate the method for estimating the spurious track background and the relative difference between the estimates is assigned as a systematic uncertainty. Excellent agreement is seen between the two control regions in both

the spurious track probability and the spurious track estimate itself, with the estimates agreeing to within ≈8% for the 2016 data, and this is taken as a systematic uncertainty. Again, both estimates are zero in the 2015 data, but without any indication their behaviors are different from 2016 data, we assign a 20% systematic uncertainty for this period and implement this as in Ref. [41].

6.2 Signal efficiency

Theoretical uncertainties of 3–9% (depending on the chargino mass) that include factorization and renormalization scale uncertainties as well as the PDF uncertainties are assigned to the chargino production cross sections. Additional sources of systematic uncertainty in the signal yields include those in the integrated luminosity, 2.3 (2.5)% for 2015 (2016) data [16, 17], and those related to the modeling of pileup (2–3%), ISR (8–9%), jet energy scale and resolution (2–6%), and $p_{\mathrm{T}}^{\mathrm{miss}}$ (0.4%), with the exact values of these uncertainties depending on chargino mass and lifetime. We also estimate uncertainties in the efficiency of the selection criteria on missing inner, middle, and outer hits (1–3%, 0.3–3%, and 0.03–3%, respectively), and E_{calo} (0.6–1%), with exact values that depend on the run period being considered. We evaluate uncertainties to account for potential mismodeling of the trigger efficiency (4–6%, depending on chargino mass and lifetime) and track reconstruction efficiency, namely, 1.5 (4.5)% for 2015 (2016) data. The systematic uncertainties in the signal yields are summarized in Table 3.

Table 3: Summary of the systematic uncertainties in the signal yields. The ranges represent either the variation with chargino mass and lifetime or with the data-taking period used to calculate the uncertainty, depending on the source of each uncertainty as described in the text.

Source of uncertainty	Typical value
Integrated luminosity	2.3–2.5%
Pileup	2–3%
ISR	8–9%
Jet energy scale/resolution	2–6%
$p_{\mathrm{T}}^{\mathrm{miss,\,no}\,\mu}$ modeling	0.4%
Missing inner hits	1–3%
Missing middle hits	0.3–3%
Missing outer hits	0.03–3%
E_{calo} selection	0.6–1%
Trigger efficiency	4–6%
Track reconstruction efficiency	1.5–4.5%
Total	10–16%

7 Results

The numbers of expected events from background sources compared with the observed numbers of events in the search sample are shown in Table 4. The observation agrees with the expected background. We set 95% CL upper limits on the product of the cross section of direct chargino production and branching fraction to $\widetilde{\chi}_1^0\pi^{\pm}$ for various chargino masses and lifetimes.

These limits are calculated using the LHC-type [42] modified frequentist $\mathrm{CL_s}$ criterion [43, 44]. This method uses a test statistic based on a profile likelihood ratio [45] and treats nuisance parameters in a frequentist context. Nuisance parameters for the theoretical uncertainties in the

Table 4: Summary of numbers of events for the estimated backgrounds and the observed data. The uncertainties include those from statistical and systematic sources. In categories where the systematic uncertainty is negligibly small, it is not shown.

Run period	Estimated number of background events			Observed events
	Leptons	Spurious tracks	Total	
2015	0.1 ± 0.1	$0^{+0.1}_{-0}$	0.1 ± 0.1	1
2016A	$2.0 \pm 0.4 \pm 0.1$	$0.4 \pm 0.2 \pm 0.4$	$2.4 \pm 0.5 \pm 0.4$	2
2016B	$3.1 \pm 0.6 \pm 0.2$	$0.9 \pm 0.4 \pm 0.9$	$4.0 \pm 0.7 \pm 0.9$	4
Total	$5.2 \pm 0.8 \pm 0.3$	$1.3 \pm 0.4 \pm 1.0$	$6.5 \pm 0.9 \pm 1.0$	7

signal cross sections and systematic uncertainties in the integrated luminosity and in the signal selection efficiency are constrained with log-normal distributions. There are two types of nuisance parameters for the uncertainties in the background estimates, and they are specified separately for each of the four background contributions. Those that result from the limited size of the control samples are constrained with gamma distributions, while those that are associated with statistical uncertainties in multiplicative factors and the systematic uncertainties discussed in Section 6 are constrained with log-normal distributions.

The expected and observed limits on the product of the direct chargino production cross section (σ) and branching fraction to $\widetilde{\chi}^0_1\pi^\pm$ ($\mathcal{B}$) are shown in Fig. 3 as a function of chargino mass for several different chargino lifetimes. The direct chargino production cross section includes both $\widetilde{\chi}^0_1\widetilde{\chi}^\pm_1$ and $\widetilde{\chi}^\pm_1\widetilde{\chi}^\mp_1$ production in roughly a 2:1 ratio across all chargino masses considered. The intersection of the theory prediction and the upper limit on the cross section is used to set a constraint on the mass of the chargino, for a given chargino lifetime. This procedure is repeated for a large number of chargino lifetimes, in order to produce a two-dimensional constraint on the chargino mass and mean proper lifetime, which is shown in Fig. 4. Charginos with a lifetime of 3 ns are excluded up to a mass of 715 GeV. Figure 5 shows the observed limits on the product of the direct chargino production cross section and branching fraction to $\widetilde{\chi}^0_1\pi^\pm$.

8 Summary

A search has been presented for long-lived charged particles that decay within the CMS detector and produce the signature of a disappearing track. In a sample of proton-proton data recorded at a center-of-mass energy of $\sqrt{s} = 13\,\text{TeV}$ and corresponding to an integrated luminosity of $38.4\,\text{fb}^{-1}$, seven events are observed in the search sample, compared with the estimated background from standard model processes of $6.5 \pm 0.9\,(\text{stat}) \pm 1.0\,(\text{syst})$ events. The observation is consistent with the background-only hypothesis, and we place constraints on the mass of charginos from direct electroweak production, for chargino mean proper lifetimes between 0.1 and 100 ns. Charginos with a mass up to 715 GeV for a lifetime of 3 ns are excluded at 95% confidence level. These constraints extend the limits set by a previous search performed by CMS [9]. For chargino lifetimes above $\approx$0.7 ns, the present search places the most stringent constraints on direct chargino production using the disappearing track signature.

Acknowledgments

We congratulate our colleagues in the CERN accelerator departments for the excellent performance of the LHC and thank the technical and administrative staffs at CERN and at other CMS institutes for their contributions to the success of the CMS effort. In addition, we grate-

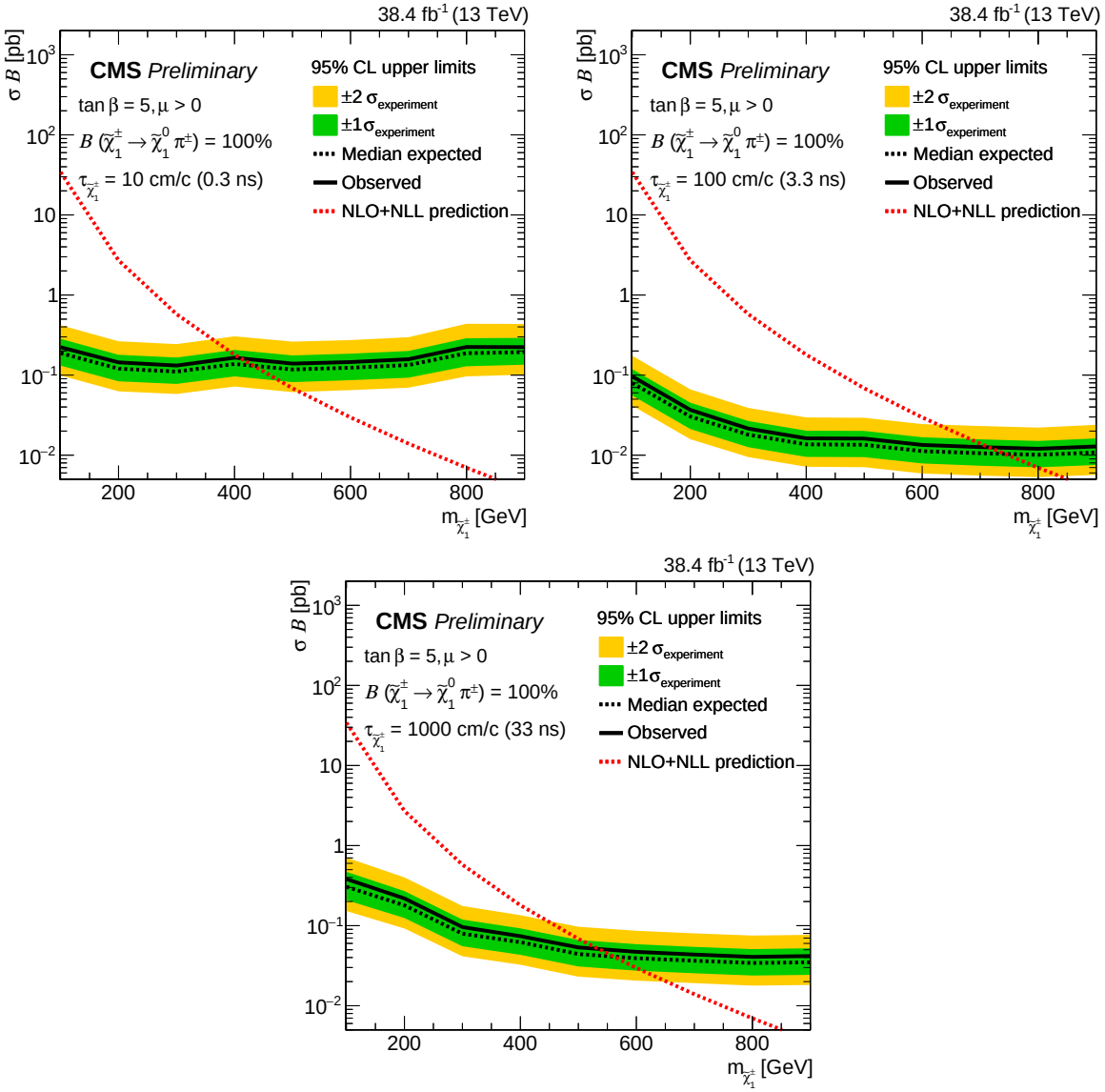

Figure 3: The expected and observed 95% CL upper limits on the product of the cross section of direct chargino production and branching fraction to $\widetilde{\chi}_1^0\pi^\pm$ as a function of chargino mass for various chargino lifetimes. The direct chargino production cross section includes both $\widetilde{\chi}_1^0\widetilde{\chi}_1^\pm$ and $\widetilde{\chi}_1^\pm\widetilde{\chi}_1^\mp$ production in roughly a 2:1 ratio across all chargino masses considered.

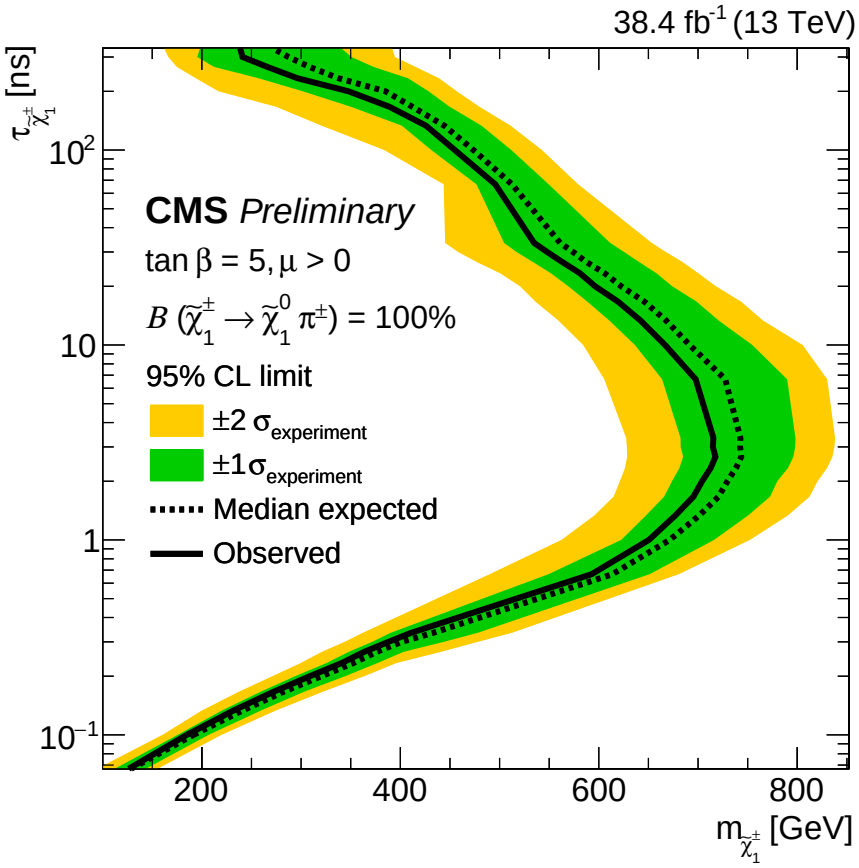

Figure 4: The expected and observed constraints on chargino lifetime and mass. The region to the left of the curve is excluded at 95% CL.

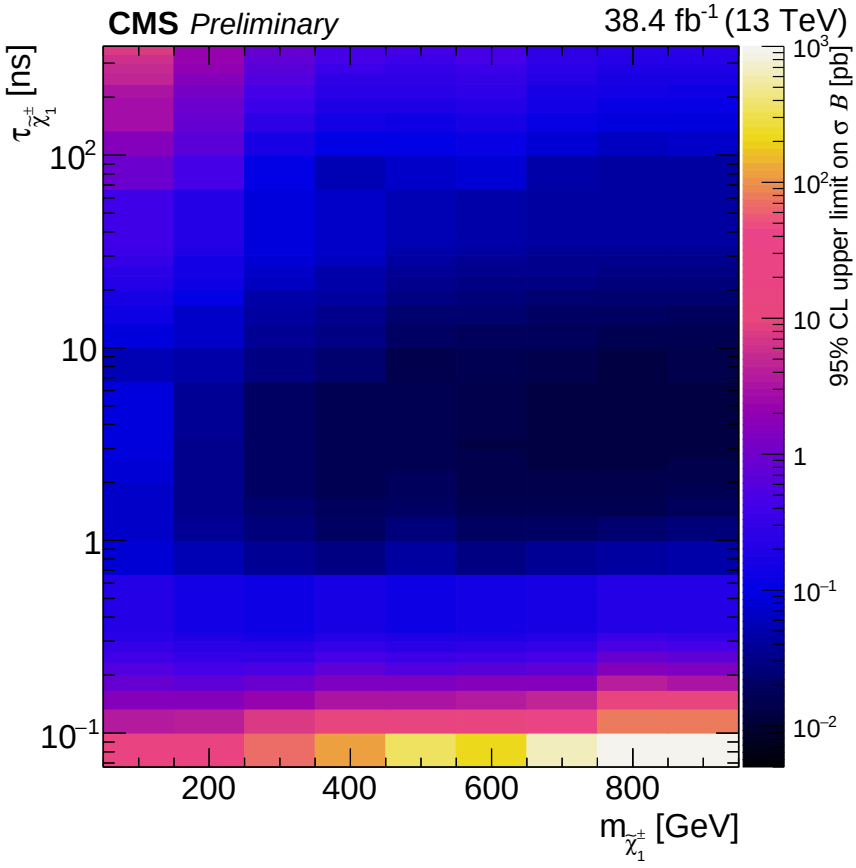

Figure 5: The observed 95% CL upper limits on the product of the cross section of direct chargino production and branching fraction to $\widetilde{\chi}_1^0\pi^\pm$ as a function of chargino mass and lifetime. The direct chargino production cross section includes both $\widetilde{\chi}_1^0\widetilde{\chi}_1^\pm$ and $\widetilde{\chi}_1^\pm\widetilde{\chi}_1^\mp$ production in roughly a 2:1 ratio across all chargino masses considered.

fully acknowledge the computing centres and personnel of the Worldwide LHC Computing Grid for delivering so effectively the computing infrastructure essential to our analyses. Finally, we acknowledge the enduring support for the construction and operation of the LHC and the CMS detector provided by the following funding agencies: BMWFW and FWF (Austria); FNRS and FWO (Belgium); CNPq, CAPES, FAPERJ, and FAPESP (Brazil); MES (Bulgaria); CERN; CAS, MoST, and NSFC (China); COLCIENCIAS (Colombia); MSES and CSF (Croatia); RPF (Cyprus); SENESCYT (Ecuador); MoER, ERC IUT, and ERDF (Estonia); Academy of Finland, MEC, and HIP (Finland); CEA and CNRS/IN2P3 (France); BMBF, DFG, and HGF (Germany); GSRT (Greece); OTKA and NIH (Hungary); DAE and DST (India); IPM (Iran); SFI (Ireland); INFN (Italy); MSIP and NRF (Republic of Korea); LAS (Lithuania); MOE and UM (Malaysia); BUAP, CINVESTAV, CONACYT, LNS, SEP, and UASLP-FAI (Mexico); MBIE (New Zealand); PAEC (Pakistan); MSHE and NSC (Poland); FCT (Portugal); JINR (Dubna); MON, RosAtom, RAS, RFBR and RAEP (Russia); MESTD (Serbia); SEIDI, CPAN, PCTI and FEDER (Spain); Swiss Funding Agencies (Switzerland); MST (Taipei); ThEPCenter, IPST, STAR, and NSTDA (Thailand); TUBITAK and TAEK (Turkey); NASU and SFFR (Ukraine); STFC (United Kingdom); DOE and NSF (USA).

Individuals have received support from the Marie-Curie programme and the European Research Council and Horizon 2020 Grant, contract No. 675440 (European Union); the Leventis Foundation; the A. P. Sloan Foundation; the Alexander von Humboldt Foundation; the Belgian Federal Science Policy Office; the Fonds pour la Formation à la Recherche dans l'Industrie et dans l'Agriculture (FRIA-Belgium); the Agentschap voor Innovatie door Wetenschap en Technologie (IWT-Belgium); the F.R.S.-FNRS and FWO (Belgium) under the "Excellence of Science - EOS" - be.h project n. 30820817; the Ministry of Education, Youth and Sports (MEYS) of the Czech Republic; the Council of Science and Industrial Research, India; the HOMING PLUS programme of the Foundation for Polish Science, cofinanced from European Union, Regional Development Fund, the Mobility Plus programme of the Ministry of Science and Higher Education, the National Science Center (Poland), contracts Harmonia 2014/14/M/ST2/00428, Opus 2014/13/B/ST2/02543, 2014/15/B/ST2/03998, and 2015/19/B/ST2/02861, Sonata-bis 2012/07/E/ST2/01406; the National Priorities Research Program by Qatar National Research Fund; the Programa Severo Ochoa del Principado de Asturias; the Thalis and Aristeia programmes cofinanced by EU-ESF and the Greek NSRF; the Rachadapisek Sompot Fund for Postdoctoral Fellowship, Chulalongkorn University and the Chulalongkorn Academic into Its 2nd Century Project Advancement Project (Thailand); the Welch Foundation, contract C-1845; and the Weston Havens Foundation (USA).

References

[1] G. F. Giudice, M. A. Luty, H. Murayama, and R. Rattazzi, "Gaugino mass without singlets", *JHEP* **12** (1998) 027, doi:10.1088/1126-6708/1998/12/027, arXiv:hep-ph/9810442.

[2] L. Randall and R. Sundrum, "Out of this world supersymmetry breaking", *Nucl. Phys. B* **557** (1999) 79, doi:10.1016/S0550-3213(99)00359-4, arXiv:hep-th/9810155.

[3] C. H. Chen, M. Drees, and J. F. Gunion, "A nonstandard string / SUSY scenario and its phenomenological implications", *Phys. Rev. D* **55** (1997) 330, doi:10.1103/PhysRevD.55.330, arXiv:hep-ph/9607421. [Erratum: doi:10.1103/PhysRevD.60.039901].

[4] M. Ibe, S. Matsumoto, and T. T. Yanagida, "Pure gravity mediation with $m_{3/2} = 10$–100 TeV", *Phys. Rev. D* **85** (2012) 095011, doi:10.1103/PhysRevD.85.095011, arXiv:1202.2253.

[5] L. J. Hall, Y. Nomura, and S. Shirai, "Spread supersymmetry with wino LSP: gluino and dark matter signals", *JHEP* **01** (2013) 036, doi:10.1007/JHEP01(2013)036, arXiv:1210.2395.

[6] A. Arvanitaki, N. Craig, S. Dimopoulos, and G. Villadoro, "Mini-split", *JHEP* **02** (2013) 126, doi:10.1007/JHEP02(2013)126, arXiv:1210.0555.

[7] N. Arkani-Hamed et al., "Simply unnatural supersymmetry", (2012). arXiv:1212.6971.

[8] M. Citron et al., "End of the CMSSM coannihilation strip is nigh", *Phys. Rev. D* **87** (2013) 036012, doi:10.1103/PhysRevD.87.036012, arXiv:1212.2886.

[9] CMS Collaboration, "Search for disappearing tracks in proton-proton collisions at $\sqrt{s} = 8$ TeV", *JHEP* **01** (2015) 096, doi:10.1007/JHEP01(2015)096, arXiv:1411.6006.

[10] ATLAS Collaboration, "Search for charginos nearly mass degenerate with the lightest neutralino based on a disappearing-track signature in pp collisions at $\sqrt{s}$ = 8 TeV with the ATLAS detector", *Phys. Rev. D* **88** (2013) 112006, doi:10.1103/PhysRevD.88.112006, arXiv:1310.3675.

[11] ATLAS Collaboration, "Search for long-lived charginos based on a disappearing-track signature in pp collisions at $\sqrt{s}$ = 13 TeV with the ATLAS detector", (2017). arXiv:1712.02118. Submitted to *JHEP*.

[12] CMS Collaboration, "Description and performance of track and primary-vertex reconstruction with the CMS tracker", *JINST* **9** (2014) P10009, doi:10.1088/1748-0221/9/10/P10009, arXiv:1405.6569.

[13] CMS Collaboration, "The CMS trigger system", *JINST* **12** (2017) P01020, doi:10.1088/1748-0221/12/01/P01020, arXiv:1609.02366.

[14] CMS Collaboration, "Particle-flow reconstruction and global event description with the CMS detector", *JINST* **12** (2017) P10003, doi:10.1088/1748-0221/12/10/P10003, arXiv:1706.04965.

[15] CMS Collaboration, "The CMS experiment at the CERN LHC", *JINST* **3** (2008) S08004, doi:10.1088/1748-0221/3/08/S08004.

[16] CMS Collaboration, "CMS luminosity measurement for the 2015 data taking period", CMS Physics Analysis Summary CMS-PAS-LUM-15-001, 2016.

[17] CMS Collaboration, "CMS luminosity measurements for the 2016 data taking period", CMS Physics Analysis Summary CMS-PAS-LUM-17-001, 2017.

[18] T. Sjöstrand, S. Mrenna, and P. Z. Skands, "PYTHIA 6.4 physics and manual", *JHEP* **05** (2006) 026, doi:10.1088/1126-6708/2006/05/026, arXiv:hep-ph/0603175.

[19] J. Pumplin et al., "New generation of parton distributions with uncertainties from global QCD analysis", *JHEP* **07** (2002) 012, doi:10.1088/1126-6708/2002/07/012, arXiv:hep-ph/0201195.

[20] F. E. Paige, S. D. Protopopescu, H. Baer, and X. Tata, "ISAJET 7.69: A Monte Carlo event generator for pp, $\overline{\text{p}}$p, and e^+e^- reactions", (2003). arXiv:hep-ph/0312045.

[21] B. Fuks, M. Klasen, D. R. Lamprea, and M. Rothering, "Gaugino production in proton-proton collisions at a center-of-mass energy of 8 TeV", *JHEP* **10** (2012) 081, doi:10.1007/JHEP10(2012)081, arXiv:1207.2159.

[22] B. Fuks, M. Klasen, D. R. Lamprea, and M. Rothering, "Precision predictions for electroweak superpartner production at hadron colliders with RESUMMINO", *Eur. Phys. J. C* **73** (2013) 2480, doi:10.1140/epjc/s10052-013-2480-0, arXiv:1304.0790.

[23] P. M. Nadolsky et al., "Implications of CTEQ global analysis for collider observables", *Phys. Rev. D* **78** (2008) 013004, doi:10.1103/PhysRevD.78.013004, arXiv:0802.0007.

[24] A. D. Martin, W. J. Stirling, R. S. Thorne, and G. Watt, "Parton distributions for the LHC", *Eur. Phys. J. C* **63** (2009) 189, doi:10.1140/epjc/s10052-009-1072-5, arXiv:0901.0002.

[25] J. Alwall et al., "MadGraph 5: going beyond", *JHEP* **06** (2011) 128, doi:10.1007/JHEP06(2011)128, arXiv:1106.0522.

[26] J. Alwall et al., "The automated computation of tree-level and next-to-leading order differential cross sections, and their matching to parton shower simulations", *JHEP* **07** (2014) 079, doi:10.1007/JHEP07(2014)079, arXiv:1405.0301.

[27] T. Sjöstrand, S. Mrenna, and P. Z. Skands, "A brief introduction to PYTHIA 8.1", *Comput. Phys. Commun.* **178** (2008) 852, doi:10.1016/j.cpc.2008.01.036, arXiv:0710.3820.

[28] P. Nason, "A new method for combining NLO QCD with shower Monte Carlo algorithms", *JHEP* **11** (2004) 040, doi:10.1088/1126-6708/2004/11/040, arXiv:hep-ph/0409146.

[29] S. Frixione, P. Nason, and C. Oleari, "Matching NLO QCD computations with parton shower simulations: the POWHEG method", *JHEP* **11** (2007) 070, doi:10.1088/1126-6708/2007/11/070, arXiv:0709.2092.

[30] S. Alioli, P. Nason, C. Oleari, and E. Re, "A general framework for implementing NLO calculations in shower Monte Carlo programs: the POWHEG BOX", *JHEP* **06** (2010) 043, doi:10.1007/JHEP06(2010)043, arXiv:1002.2581.

[31] T. Melia, P. Nason, R. Rontsch, and G. Zanderighi, "W^+W^-, WZ and ZZ production in the POWHEG BOX", *JHEP* **11** (2011) 078, doi:10.1007/JHEP11(2011)078, arXiv:1107.5051.

[32] P. Nason and G. Zanderighi, "W^+W^-, WZ and ZZ production in the POWHEG-BOX-V2", *Eur. Phys. J. C* **74** (2014) 2702, doi:10.1140/epjc/s10052-013-2702-5, arXiv:1311.1365.

[33] NNPDF Collaboration, "Parton distributions for the LHC Run II", *JHEP* **04** (2015) 040, doi:10.1007/JHEP04(2015)040, arXiv:1410.8849.

[34] P. Skands, S. Carrazza, and J. Rojo, "Tuning PYTHIA 8.1: the Monash 2013 tune", *Eur. Phys. J. C* **74** (2014) 3024, doi:10.1140/epjc/s10052-014-3024-y, arXiv:1404.5630.

[35] CMS Collaboration, "Event generator tunes obtained from underlying event and multiparton scattering measurements", *Eur. Phys. J. C* **76** (2016) 155, doi:10.1140/epjc/s10052-016-3988-x, arXiv:1512.00815.

[36] GEANT4 Collaboration, "GEANT4 — a simulation toolkit", *Nucl. Instrum. Meth. A* **506** (2003) 250, doi:10.1016/S0168-9002(03)01368-8.

[37] M. Cacciari, G. P. Salam, and G. Soyez, "FastJet user manual", *Eur. Phys. J. C* **72** (2012) 1896, doi:10.1140/epjc/s10052-012-1896-2, arXiv:1111.6097.

[38] M. Cacciari, G. P. Salam, and G. Soyez, "The anti-k_t jet clustering algorithm", *JHEP* **04** (2008) 063, doi:10.1088/1126-6708/2008/04/063, arXiv:0802.1189.

[39] CMS Collaboration, "Jet algorithms performance in 13 TeV data", CMS Physics Analysis Summary CMS-PAS-JME-16-003, 2017.

[40] Particle Data Group Collaboration, "Review of particle physics", *Chin. Phys. C* **40** (2016) 100001, doi:10.1088/1674-1137/40/10/100001.

[41] R. D. Cousins and V. L. Highland, "Incorporating systematic uncertainties into an upper limit", *Nucl. Instrum. Meth. A* **320** (1992) 331, doi:10.1016/0168-9002(92)90794-5.

[42] The ATLAS Collaboration, The CMS Collaboration, The LHC Higgs Combination Group, "Procedure for the LHC Higgs boson search combination in summer 2011", Technical Report ATL-PHYS-PUB-2011-011, CMS-NOTE-2011-005, 2011.

[43] A. L. Read, "Presentation of search results: The CL_s technique", *J. Phys. G* **28** (2002) 2693, doi:10.1088/0954-3899/28/10/313.

[44] T. Junk, "Confidence level computation for combining searches with small statistics", *Nucl. Instrum. Meth. A* **434** (1999) 435, doi:10.1016/S0168-9002(99)00498-2, arXiv:hep-ex/9902006.

[45] G. Cowan, K. Cranmer, E. Gross, and O. Vitells, "Asymptotic formulae for likelihood-based tests of new physics", *Eur. Phys. J. C* **71** (2011) 1554, doi:10.1140/epjc/s10052-011-1554-0, arXiv:1007.1727. [Erratum: doi:10.1140/epjc/s10052-013-2501-z].